Simulations of ground moving target indication in an ultra-wideband and wide-beam SAR system

Mats I. Pettersson*, Lars M.H. Ulander, Hans Hellsten
Swedish Defence Research Establishment, Division of Sensor Technology.
P.O. Box 1165, SE-581 11 Linköping, Sweden

ABSTRACT

This paper discusses the methods for ground moving target indication (GMTI) in a bistatic ultra-wideband and wide-beam (UWB-WB) SAR system. Simulations of GMTI in UWB-WB SAR system are shown. Bistatic compensation in a time domain SAR processing system is given, and clutter leakage caused by bistatic radar and time domain fast backprojection SAR algorithms is studied. The clutter leakage is investigated both for the scatter and for the sidlobes of the scatter.

In the paper we also discuss clutter leakage caused by bistatic scattering. As the scatter size increases the bistatic wave will scatter differently then the monostatic wave. Also the effect of bistatic nadir and antenna configuration is studied.

Keywords: SAR, UWB, GMTI, bistatic, clutter leakage, fast backprojection, VHF, UHF, scattering, simulations

1. INTRODUCTION

This paper discusses methods for detection, localization, and velocity determination of moving targets in bistatic ultra-wideband and wide-beam (UWB-WB) Synthetic Aperture Radar (SAR) system.

The purpose of moving target indication (MTI) radar is to reject signals from fixed or slow moving unwanted targets, such as buildings, trees and sea, and retain moving targets such as trucks, aircraft and boats for detection. In MTI the Doppler information of the moving target is separated from the Doppler information of the clutter. In ground moving target indication (GMTI) slow moving targets which do not have separated Doppler information are also detected.

Because the traditional MTI systems gave bad performance for slow ground moving targets there has in the latest years been an increased interest on GMTI in a synthetic aperture radar (SAR) system[1,2]. The SAR system adds the possibility to obtain high resolution radar. However, without GMTI, standard SAR processing may cause the moving target to disappear, through defocusing, or may be confused with a static target, displaced in azimuth due to the ambiguity between bearing and target speed. These effects of moving targets in a SAR system were first investigated by Raney[3]. To solve this ambiguity for a SAR-GMTI system there are different methods, we have in this paper used a multiple antenna phase center method. The idea with many antenna channels is to measure at the same position in space but at different occasions in time.

In this paper we discuss the aspects of GMTI in a UWB-WB radar system. The common situation is that the target is hidden by the ground clutter and that the target is moving. To increase target to clutter ratio the radar signal is filtered. The main idea of the clutter filter is that the clutter is stable in time while a moving target is not. In particular at low frequencies the clutter will be stable, because the objects which cause the reflection have a physical size. As an example in forests it is not the leaves, or branches which cause the reflection but rather the stable ground-trunk which is the major backscatter contributor[4].

With GMTI at low frequencies, such as VHF (30-300MHz) or UHF (300MHz-1GHz), together with a UWB-WB SAR system we add a lot of new possibilities. The low frequency provide capability of foliage penetration for detecting concealed targets. It has been shown that a VHF SAR sensor provides a combination of low foliage backscattering coefficient with a low two-way attenuation value. This means that a UWB VHF SAR system has an improved target to clutter ratio, and in particular, change detection has been shown to be a powerful detection method for concealed targets[5]. Furthermore, low frequencies is a straight forward technique to detect stealth-designed targets. It is the aim of this work to study the performance of GMTI in a UWB-WB low frequency SAR system.

2. THE GMTI SYSTEM

2.1. The GMTI SAR overview

There are different methods to perform GMTI in SAR. The main idea in systems with more than one antenna channel is to compare radar data at the same place in space but at different points in time. As the platform moves each antenna phase

*Correspondance: Email: matsp@lin.foa.se; WWW:http://www.foa.se/carabas.html; Telephone: (+46) 13 37 80 43; Fax: (+46) 13 37 81 00

Part of the SPIE Conference on Radar Processing, Technology, and Applications IV • Denver, Colorado • July 1999
SPIE Vol. 3810 • 0277-786X/99/$10.00

center will pass the same place but they will pass it for different times, i.e. displaced phase-center antenna (DPCA). The clutter is assumed to be the same independent of time, but the moving targets will change their positions.

Because of the linear nature of the SAR process, it is possible to change order of the different processing steps. Two processors to discover moving targets is shown in Fig. 1a-1b, and they should in principal give the same results. In MTI-SAR (Fig. 1a) the GMTI filter is implemented in the range compressed data. In SAR-MTI (Fig. 1b) however, the GMTI filtering is done in SAR processed data.

The system in Fig. 1a-1b is a three antenna system, and all channels are pulse compressed to the G signals. For MTI-SAR the G signals are used to determine the MTI filtered M signals. The signals SM1 and SM2 are the SAR processed MTI filtered M1 and M2 signals. The moving target parameters are estimated from SM_{corr} which is the correlation between SM1 and SM2. To focus a moving target the SAR process has to be performed for the correct relative speed[6,7]. For the SAR-MTI, images X1 and X2 both contain moving and the non-moving targets. The non-moving targets are filtered after SAR processing.

To estimate the movement of the target detected by the first MTI channel we need a second channel. The second GMTI channels SM2 and MS2 are formed from G2 and G3. Because images MS1 and SM1 are measured some time before MS2 and SM2 the displacement can be measured by correlation of the two signals.

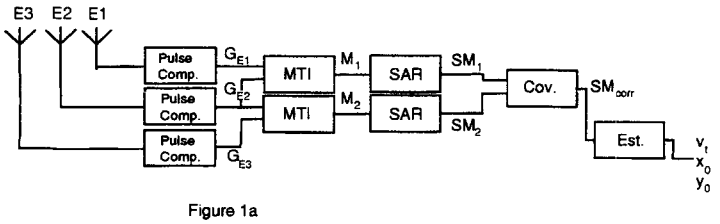

Figure 1a

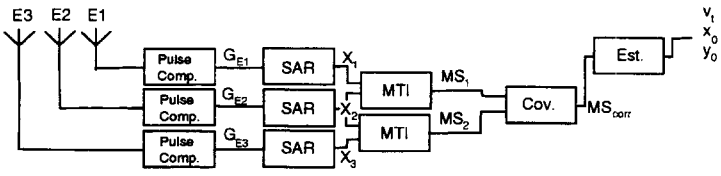

Figure 1b

Figure 1. The SAR processors

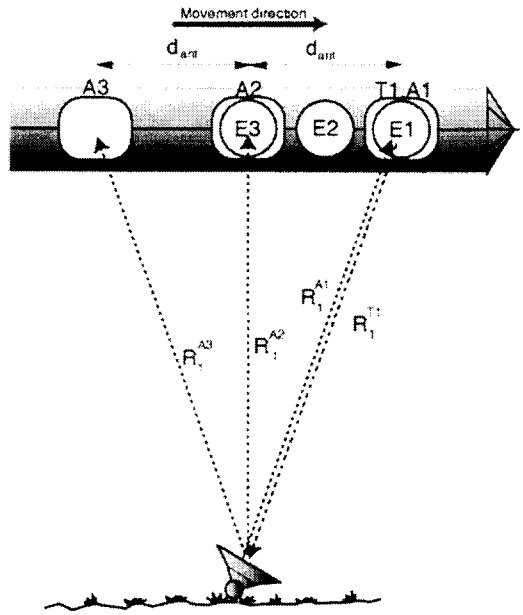

Figure 2. The antenna system

2.2. The antenna system

A possible antenna system for a SAR with GMTI capability is shown in Fig. 2. The antenna elements A1, A2, and A3 are located on a line oriented in the main platform movement direction. Because we are most interested in low frequency systems the antenna element separation may by so large, that A1 is in the front of an airplane and A3 in the back.

To save time one antenna element is transmitting and three are receiving. We assume that the antenna element T1 (same as element A1) transmits a pulse, and after time $2R_1/c$, $(R_1+R_2)/c$ and $(R_1+R_3)/c$ the receiving elements A1, A2 and A3 receive the back scattered signal from the target. Antenna A1 is a monostatic channel, whereas A2 and A3, are bistatic channels. Although the antenna-target distances are not the same for the bistatic channels as for the monostatic channel, we will for simplicity form effective antenna centers. The effective antenna centers E1, E2 and E3 are imaginary antennas located in the middle of the receiving and transmitting antennas, one for each channel. We can then imagine that the transmit and received signals originate from an equivalent monostatic antenna channel. However, the equivalence is not exact and require a small distance correction as discussed below.

3. CLUTTER CANCELLATION AND MOVING TARGET DISTORTION

3.1. The Monostatic Radar-Circular Geometry

For simplicity we first study the case of two monostatic antennas. Each range signal will form a circular footprint in the slant-range plane and on the ground. This means that in an ideal wide-beam antenna system we will have backscattering

contributions from all directions on the half circle. To notch the clutter we have to use two monostatic antennas, which are subtracted after a time delay.

Fig. 3 shows one point target located at distance r_1. If the target is not moving the Doppler information is only dependent on φ_1, and the platform speed v_p. If we know the platform speed v_p we can from the Doppler information determine the angle. If, however, the target is moving with speed v_t, the Doppler information would not give the true angle φ_1 i.e. the motion will change the angle to φ_1'. This equivalence is governed by the Doppler equation

$$f_{d1} = 2f_0 \frac{v_p}{c_0}\cos\varphi_1 - 2f_0 \frac{v_t}{c_0}\hat{\mathbf{r}}_1 \cdot \hat{\mathbf{v}}_t = 2\frac{f_0}{c_0}\left(v_p \cos\varphi_1 - v_t \cos(\theta - \varphi_1)\right) \tag{1}$$

where f_0 is the frequency, and c_0 is the speed of the light.

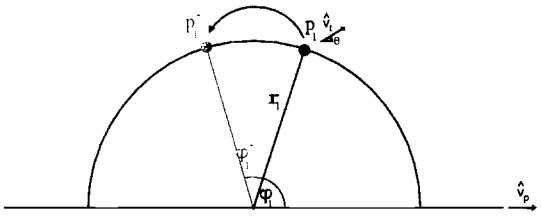

Figure 3. Monostatic radar

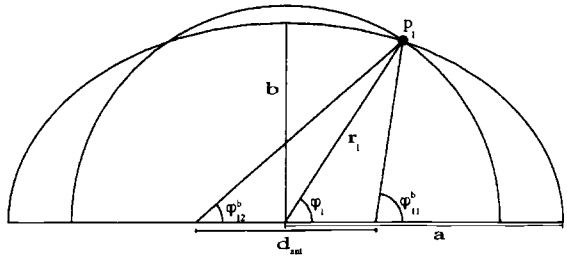

Figure 4. Monostatic and bistatic radar

3.2. The Bistatic Radar-Elliptical Geometry

If we filter the non moving targets in a system with monostatic and bistatic antennas, we have to compensate the bistatic signal to the monostatic signal. In Fig. 4 we see that the difference in distance between bistatic and monostatic at the effective antennas centers is 2a-2r. Using the geometry in Fig. 4 we find

$$\begin{aligned} a\cos t &= r_1 \cos\varphi_1 \\ b\sin t &= r_1 \sin\varphi_1 \end{aligned} \tag{2}$$

using $b^2 = a^2 - \frac{d_{ant}^2}{4}$ and by division by (2) it result in

$$r_1 = a\sqrt{\frac{4a^2 - d_{ant}^2}{4a^2 - d_{ant}^2\cos^2\varphi_1}} \tag{3}$$

If $d_{ant} << r_1$ the bistatic to the monostatic compensation is given by

$$\Delta_b = a\left(1 - \sqrt{\frac{4a^2 - d_{ant}^2}{4a^2 - d_{ant}^2\cos^2\varphi_1}}\right) \approx \frac{d_{ant}^2}{8r_1}\sin^2\varphi_1 \tag{4}$$

In a system flying at 1000 meter with a antenna separation of 40 meter, the maximum bistatic compensation is 0.2m.

3.3. Moving target in bistatic geometry

The bistatic compensation in (5) is dependent on the angle to the target, and the angle measurement relies on the Doppler information. If we know our velocity, non moving targets can be compensated. But what happens when the target is moving with unknown speed. We investigate this measurement error in a monostatic-bistatic system.

The geometry of the system is illustrated in Fig. 5. We position the target in point p_2, i.e. its bistatic range is $2a_2$. The target Doppler frequency makes the system believe that the target is a non moving target at the same bistatic range but with a Doppler angle φ_2'', and not as φ_2 for point two. After bistatic to monostatic compensation we will place this target at p_2'' and not p_2' as in the monostatic system. The separation between the two points is the error due to bistatic compensation. We will now express the error in terms of the monostatic system, i.e.

$$\varphi_2'' = \arccos\left\{ \cos\varphi_2 - \frac{v_t}{2v_p}\left(\cos\left(\theta - \varphi_{22}^b\right) + \cos\left(\theta - \varphi_{21}^b\right)\right)\right\} \tag{5}$$

and as in (4) the point p'' has the distance

$$r_2'' = a_2\sqrt{\frac{4a_2^2 - d_{ant}^2}{4a_2^2 - d_{ant}^2\cos^2\varphi_2''}} \tag{6}$$

If $d_{ant} << r_2$ and using Taylor expansion we get

$$\varphi_2'' \approx \arccos\left\{ \cos\varphi_2 - \frac{v_t}{v_p}\cos\left(\theta - \varphi_2\right)\right\} \tag{7}$$

$$r_2'' \approx r_2 + \frac{d_{ant}^2}{8r_2}\frac{v_t}{v_p}\cos\left(\theta - \varphi_2\right)\left\{ \cos\varphi_2 - \frac{v_t}{v_p}\cos\left(\theta - \varphi_2\right)\right\} \tag{8}$$

so the error in the velocity estimation will be

$$\frac{d_{ant}v_t}{16r_2}\cos\left(\theta - \varphi_2\right)\left\{ \cos\varphi_2 - \frac{v_t}{v_p}\cos\left(\theta - \varphi_2\right)\right\} \tag{9}$$

for d_{ant}=40 meter, r=1000 meter v_t=50 m/s, the error will be of the order of 0.2 m/s.

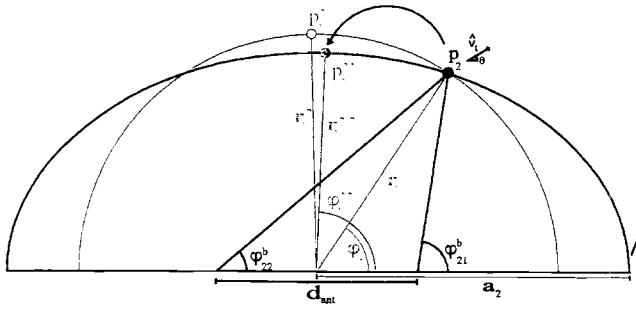

Figure 5. Moving target in monostatic-bistatic system

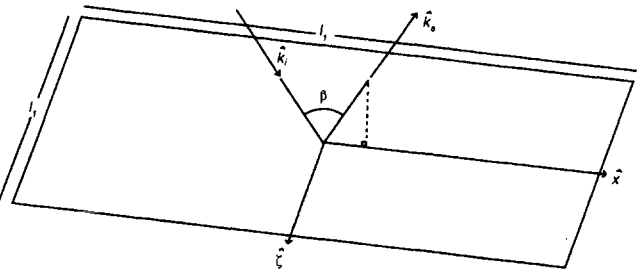

Figure 6. Scattering from a square

4. THE BACKSCATTERING IN BISTATIC RADAR

In this section, we investigate the difference in backscatter between the bistatic and monostatic case. Although a perfect range compensation for the bistatic to the monostatic case is performed, there will be a residual difference due to scattering changes.

4.1 Clutter target in monostatic and bistatic channels

To suppress clutter the scattering of the clutter has to be equal for the monostatic and the bistatic wave. However, this is only true for clutter stemming from point scatters. For other clutter the monostatic radar cross section differs from the bistatic radar cross section and the difference increases as the size of the clutter scatters increases. To study the scatter size effect, we use clutter existing of a square scatter considerably larger than the wavelength, Fig. 6. The normal of the square is antiparallel to the monostatic wave vector, and one side of the square is parallel to the azimuth direction. If the antenna separation d_{ant} in the bistatic channel is much smaller than the distance to the scatter the opening angle of the bistatic system would be

$$\beta \approx 2\arctan\left(\frac{d_{ant}\sin\varphi}{2\rho_0}\right) \tag{10}$$

The scatter will have a main scattering beamwidth of approximately

$$\alpha \approx \frac{\lambda}{l_1} \tag{11}$$

where l_1 is the length of the backscattering object. If the clutter suppression should be sufficient β has to be substantially smaller than α and therefore

$$d_{ant} << 2\rho_0 \tan\left(\frac{\lambda}{2l_1}\right) \tag{12}$$

To estimate the difference in radar cross section between the monostatic and bistatic wave we use physical optics. The radar cross section of the square[8] in Fig. 6 is given by

$$\sigma = \sigma_c \operatorname{sinc}^2\left(\frac{k_0 l_1}{2}\left(\hat{k}_i - \hat{k}_s\right)\cdot\hat{x}\right)\operatorname{sinc}^2\left(\frac{k_0 l_1}{2}\left(\hat{k}_i - \hat{k}_s\right)\cdot\hat{\zeta}\right) \tag{13}$$

where the $\hat{k}_i$ and $\hat{k}_s$ are the incidence and the observation direction, $\sigma_c = {l_1^4}/{\lambda^2}$ and k_0 the wave number. Let us for simplicity assume that the monostatic scattering occurs at maximum reflection $\sigma = \sigma_c$, e.g. the $\hat{k}_i$ and $\hat{k}_s$ are parallel to the normal of the square. Then the ratio between the bistatic and the monostatic wave will be

$$\operatorname{sinc}^2\left(\frac{k_0 l_1}{2}\left(\hat{k}_i - \hat{k}_s\right)\cdot\hat{x}\right) = \operatorname{sinc}^2\left(\frac{\pi l_1}{\lambda}\sin\frac{\beta}{2}\right) \tag{14}$$

If we assume VHF and l_1 to be 5λ=30m, d_{ant}=40m and ρ_0=1 km the ratio between the monostatic and bistatic wave will be 1.5dB. However by operating the system at larger distances the ratio improves. The same scatter will have a monostatic-bistatic ratio of 0.15dB at ρ_0=3 km. For near broad side of the target the normalized difference can be approximated as

$$\left(1 - \operatorname{sinc}^2\left(\frac{\pi l_1}{\lambda}\sin\frac{\beta}{2}\right)\right) \approx \left[\begin{array}{l} \frac{\pi l_1}{\lambda}\sin\frac{\beta}{2} << 1 \\ {d_{ant}}/{\rho_0} << 1 \end{array}\right] \approx \frac{2}{3}\left(\frac{\pi l_1}{\lambda}\frac{d_{ant}}{\rho_0}\sin\varphi\right)^2 \tag{15}$$

which means that the radar cross section ratio is dependent of the square of the distance, clutter target size and the antenna separation. For clutter targets smaller then the wavelength, the physical optics will not be valid. However for small scatters the main scattering beam α will be wider than given by (11), and therefore the ratio between monostatic and bistatic will be closer to one than (14).

4.2 The nadir reflection

The nadir reflection is the strongest single scatter in a wide-beam antenna system. The reflection coefficient for the bistatic and the monostatic wave is

$$R^b = \frac{\eta_1\cos\left(\frac{\beta}{2}\right) - \eta_2\sqrt{1-\left(\frac{\eta_2}{\eta_1}\sin\left(\frac{\beta}{2}\right)\right)^2}}{\eta_1\cos\left(\frac{\beta}{2}\right) + \eta_2\sqrt{1-\left(\frac{\eta_2}{\eta_1}\sin\left(\frac{\beta}{2}\right)\right)^2}} \tag{16}$$

where η is the intrinsic impedance of the medium, β is the bistatic opening angle with β=0 for the monostatic case. Assuming a dielectric constant of $\varepsilon=20\varepsilon_0$ and d_{ant}=40 m the normalized difference between the bistatic and monostatic wave

is -40dB. However this is in some aspects a lower bound. The surface roughness and inhomogeneity will probably cause larger differences in the nadir reflection.

5. GMTI IN LOCALBACKPROJECTION

5.1. MTI filtering

In this work we focus on the bistatic effects in a UWB-WB GMTI SAR system and we do not considered additive noise. Therefore we use a simple cancellation MTI-filter which is not adaptive. In Fig. 1, for the MTI-SAR method, it means that we form the MTI signal M in the pulse compressed signals, i.e.

$$M_1(t_s,t_f) = G_{E1}\left(t_s - \frac{d_{ant}}{2v_p},t_f\right) - G_{E2}(t_s,t_f)$$
$$M_2(t_s,t_f) = G_{E2}(t_s,t_f) - G_{E3}\left(t_s + \frac{d_{ant}}{2v_p},t_f\right) \quad (17)$$

and in the SAR-MTI method we do the MTI processing one step later in the processing chain, i.e. after the SAR processing.

$$MS_1 = X_{E1} - X_{E2} \quad MS_2 = X_{E2} - X_{E3} \quad (18)$$

5.2. Synthetic aperture processing

5.2.1. Local backprojection in monostatic radar system

SAR processing in a wide-beam system requires special algorithms in order to handle extreme range migration and motion compensation. In this work we therefore use a SAR processing technique which operates in time domain, the local backprojection[9], which is fast but approximate to the exact global back projection[10]. In the local backprojection there are two approximations made: The contribution in one subaperture from one target is an integral along a straight line, and the contribution from one subaperture over one subimage will be approximately one dimensional. The global back projection for a point target in point (x_0,ρ_0) is given by

$$h(x,\rho) = \int_{-\infty}^{\infty} g\left(x', \sqrt{(x'-x_0)^2+\rho_0^2}\right)dx' \quad (19)$$

where $g(x,R)$ is the output from the radar sensor at point (x,R) given by

$$g(x,R) = \frac{p\left(R - \sqrt{(x-x_0)^2+\rho_0^2}\right)}{\sqrt{(x-x_0)^2+\rho_0^2}} \quad (20)$$

here p(R) is the compressed pulse and R is connected to t according to t=2R/c. Consider a target located in a subimage with center coordinates ρ_c and x_c. It will be integrated over N_a subapertures with center coordinate x_{na} and with equal width as the subaperture L_s.

$$h(x,\rho) = \sum_{n_a=1}^{N_a} \int_{\left(x_{n_a}-L_s/2\right)}^{\left(x_{n_a}+L_s/2\right)} g\left(x', \sqrt{(x_{n_a}-x_c)^2+\rho_c^2} + \frac{(x'-x_{n_a})(x_{n_a}-x_c)}{\left((x_{n_a}-x_c)^2+\rho_c^2\right)^{\frac{3}{2}}}\right)dx' \quad (21)$$

This expression is for a straight flight direction. Due to the time domain integration it is easy generalize this method for a curved flight path.

5.2.2. Local backprojection in bistatic radar system

Bistatic SAR processing has been by investigated by Soumekh[11]. We will now derive the bistatic local backprojection. All points in the subaperture should be compensated due to the bistatic distance shift d_{ant}. For antenna separations $d_{ant} << r_c$ the

local backprojection is easily implemented. The radar measurement will be formed of a hyperbola with a small compensation. The distance to the target is given by

$$a \approx r + \frac{d_{ant}^2}{8r}\sin^2\varphi = r + \frac{d_{ant}^2}{8r}\frac{\rho_0^2}{r^2} \tag{22}$$

The line integral in the local backprojection is modified according to

$$\sqrt{\left(x_{n_a} - x_c\right)^2 + \rho_c^2} + \frac{d_{ant}^2\rho_c^2}{8\left(\left(x_{n_a} - x_c\right)^2 + \rho_c^2\right)^{3/2}} + \frac{\left(x_{n_a} - x_c\right)\left(x' - x_{n_a}\right)}{\sqrt{\left(x_{n_a} - x_c\right)^2 + \rho_c^2}}\left(1 - \frac{3d_{ant}^2\rho_c^2}{8\left(\left(x_{n_a} - x_c\right)^2 + \rho_c^2\right)^2}\right) \tag{23}$$

The maximum of the bistatic term is found by solving the second derivation numerically and the maximum bistatic correction occur at x_{na}-x_c =ρ_0/2. The maximum line slope bistatic correction will be in a VHF MTI system

$$\frac{3d_{ant}^2\rho_0^2\left(\frac{\rho_0}{2}\right)\left(x' - x_{n_a}\right)}{8\left(\left(\frac{\rho_0}{2}\right)^2 + \rho_0^2\right)^{\frac{5}{2}}} \le \frac{\left(x' - x_{n_a}\right)}{8\cdot 3^{\frac{5}{2}}}\frac{d_{ant}^2}{\rho_0^2} = 0.03m \tag{24}$$

for d_{ant}=40, ρ_0=1000 and for subimage size 40x40m. This error is much smaller than the approximation made in the local backprojection. However if the error is not compensated the error correspond to a speed in the MTI filter

$$\frac{\left(x - x_c\right)}{8\cdot 3^{\frac{5}{2}}}\frac{d_{ant}^2}{\rho_0^2}\frac{2v_p}{d_{ant}} \approx 0.15m/s \tag{25}$$

6. CLUTTER LEAKAGE CAUSED BY BISTATIC LOCAL BACKPROJECTION

6.1. Local image

We strictly need to compensate each burst for bistatic distance shift. In local backprojection we can only compensate each burst along the radial direction for each subimage, but not to each point in the subimage. Therefore there will be a range error in the subimage given by

$$\delta_l = \Delta - \Delta_m = \frac{d_{ant}^2}{8r}\sin^2\varphi_c - \frac{d_{ant}^2}{8r_t}\sin^2\varphi_t \tag{26}$$

where r range and r_t and φ_t is the target location. By differential

$$\delta_l = \Delta_\varphi\frac{d_{ant}^2}{8r}\sin 2\varphi - \Delta_r\frac{d_{ant}^2}{8r^2}\sin^2\varphi \tag{27}$$

the maximum error is

$$\delta_l = \frac{d_{ant}^2 L_s}{4\sqrt{2}r^2} \tag{28}$$

For L_s=40m d_{ant}=40 and r_c=1000 v_p=100m/s the maximum error is 0.01m and the speed would be 0.4m/s

6.2. Clutter leakage between subimages

A strong scatter will have side lobes in the neighboring subimages. The side lobes will be bistatic compensated to the compensation of this subimage. The strongest echo in a wide-beam system is from nadir[12]. But the bistatic compensation will not be for the nadir position but for the position of the subimage. This will case an error

$$\delta_{\text{in}} = \Delta_c - \Delta_n = \frac{d_{ant}^2}{8r}\sin^2\varphi_c - \frac{d_{ant}^2}{8r_n}\sin^2\varphi_n \tag{29}$$

the φ_n is for nadir 90° and the maximum is given for large r or for φ_c=0°. The speed of the side lobes will in these subapertures be -2 m/s, assuming d_{ant}=40, h=750m, r_c=1000 and v_p=100m/s.

6.3. Ideal clutter suppression

We have now computed the distance shift connected to the bistatic nature of our antenna system. This distance shift will cause a movement in the MTI filter, and will therefore case energy leakage through the MTI filter. If we assume that we use a chirp pulse the shape of the signal leakage will look the same as a point target moving. The signal is given by

$$g_{MTI}(r') = A\frac{ce^{-4\pi\frac{f_c}{c}jr'}}{2\pi Br'}\sin\left(2\pi B\frac{r'}{c}\left(1-\frac{2|r'|}{cT_p}\right)\right) - \frac{ce^{-4\pi\frac{f_c}{c}j\left(r'-\frac{\Delta}{2}\right)}}{4\pi B(r'+\Delta)}\sin\left(2\pi B\frac{r'+\Delta}{c}\left(1-\frac{2|r'+\Delta|}{cT_p}\right)\right) \tag{30}$$

where r'=r-R, B is the bandwidth, A is constant and c is the speed of light. Let us now use this function to investigate the clutter leakage. If the range error Δ<<c/B and the pulse time T_p>>1/B the MTI signal can be approximated as

$$g_{MTI}(r') = A\frac{2\pi B}{c}\Delta e^{-4\pi\frac{f_c}{c}jr'}\left(\frac{df(x)}{dx} + j2\frac{f_c}{B}f(x)\right)\Big|_{x=\frac{2\pi B}{c}r'} \quad \text{where} \quad f(x) = \text{sinc}(x) \tag{31}$$

When f_c>>B the clutter through the MTI channel will mainly depend on the sinc function and not it's derivative. The clutter reduction will be $(2\pi\Delta f_c/c)^2$. If however the bandwidth is in the range size as the center frequency the clutter reduction will be of the same magnitude, but the signal will depend on both the sinc function and its derivate. For large r' the sinc function and its derivate decreases as 1/r'. The signal strength will then reduce by $(1/r')^2$, so at 250 meter from nadir return the nadir side lobes has decreased by 48dB and at 1000 meters 60dB. In Fig. 7 two simulations of $|g_{MTI}(r')|^2$ in (30) with different Δ is shown. We have used the CARABAS parameters and as shown in the figure the derivate of the sinc function effect the MTI channel, because the are two maximum centered around r'=0.

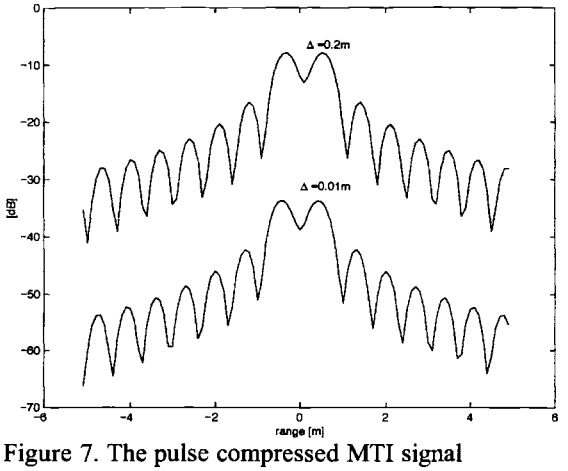

Figure 7. The pulse compressed MTI signal

7. SIMULATIONS

We now look at simulations of the different aspects of this article. We assume a system with the same radar parameters as CARABAS. The CARABAS is working on 20-90 MHz and it has a antenna diagram of a dipole antenna. The system is assumed to have three antennas channels in the along track direction according to Fig. 2, and the separation d_{ant} is 20

meters. A point target is located at the shortest range distance of 1000 meters i.e. a ground distance of 660 meters and the flight altitude is 750meters. In Fig. 8 we see the backscatted signal in the range plane of this point target. It is clear that the range migration is extreme in this wide-beam system. The wide-beam pattern will make nadir sidelobes visible. The nadir backscatter is assumed to be 40 dB stronger than the point targets, which is an experience from the CARABAS sensor.

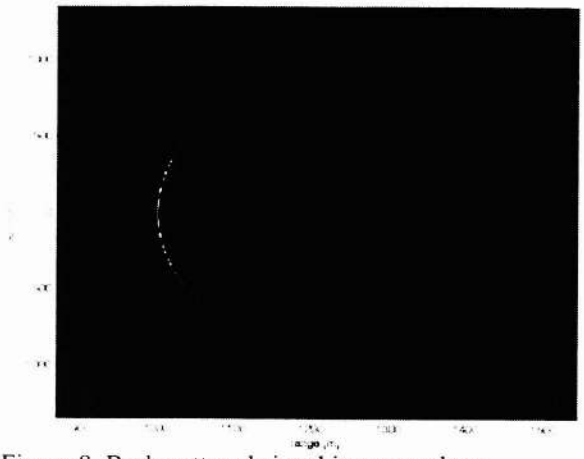

Figure 8. Backscattered signal in range plane

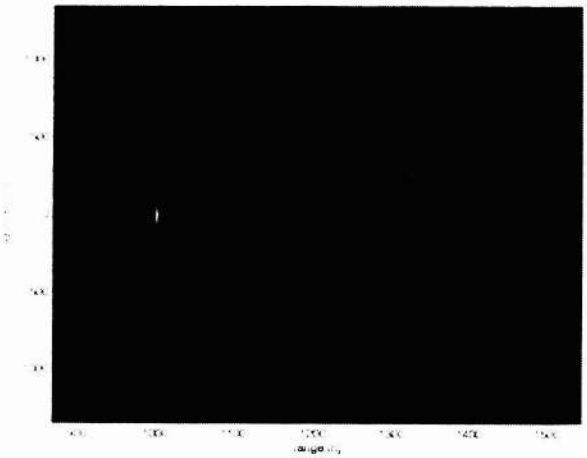

Figure 9. Backscattered signal in range plane

If more targets are present each will make an unique range migration pattern. In Fig. 9 eighteen non moving target and two moving targets are present, in the background of the figure the nadir side lobes is visible.
Using the local backprojection method for the SAR process, we will first form subaperture beams and subimages. For every subimage we will form a range vector for each subaperture. The local range vector for one subimage for all different subapertures is shown in Fig. 10. In this case there are two targets present, one at the center of the subimage and one separated 10 meters both in azimuth and range. The center target will be placed in the same position while the offset target perform a range walk in the local range vector.

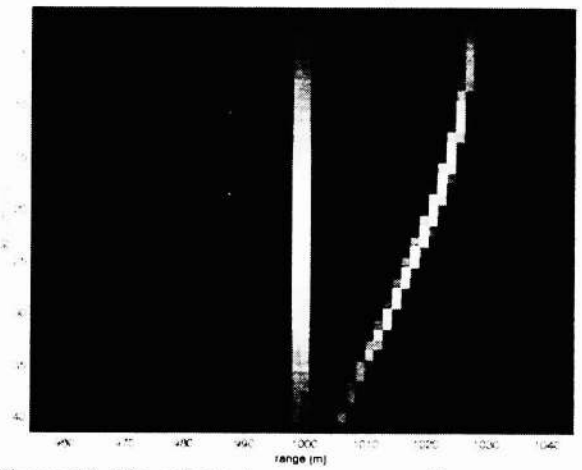

Figure 10. The subapertures over one subimage

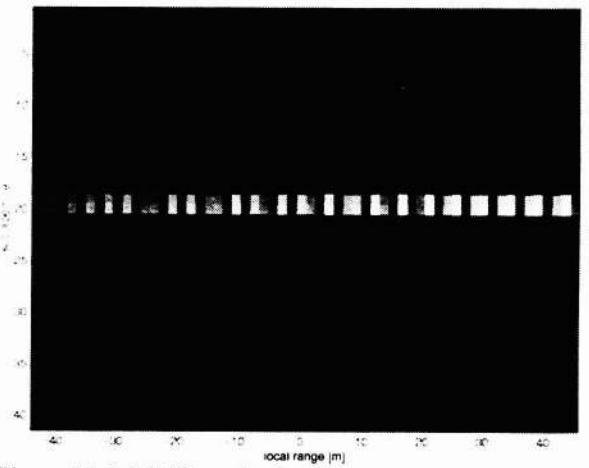

Figure 11. MTI filtered subapertures

If we choose to make MTI filtering at this stage, we are able to separate different direction to correct for the bistatic distance shift. We will compensate each burst to its bistatic error and transfer it to the local range. The local range vector can then be seen as a beam former over the subimage where angle dependence can be corrected. This is important because the antenna channels, due to different antenna patterns, also have to correct the distance cased by the bistatic nature of the system. In Fig. 11 we present the MTI filtered *M* channel. As seen the strongest signal appear in the middle, which correspond to the zero Doppler direction. From the discussion in section 6.2 it is clear that this pattern is caused by the nadir reflections side lobes. If the nadir is removed from the simulations the local range vector will look as in Fig. 12. The target in the middle of the subimage will have signal describing the distance error caused by the approximation in (4) which will case a MTI signal given by (32). The offset target will have a signal strength where the distance error is described in (27). The error caused by the local image is small when the radial direction is in the direction of the direction between the local image

center and the target. However as the radial direction changes from this direction the error increases, and therefore the signal strength.

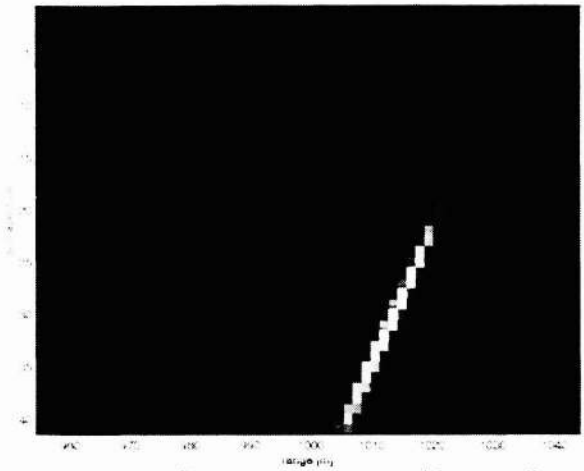

Figure 12. MTI filtered subapertures without nadir

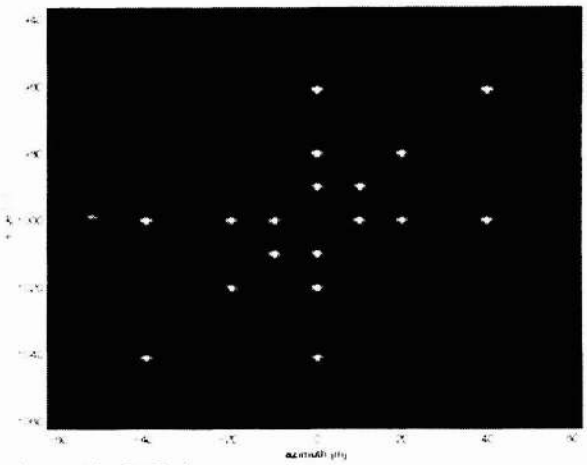

Figure 13. SAR image

From the subaperture range vectors it is now possible to process the SAR image. We first show the SAR image from one channel, Fig. 13. In this case we have 18 non moving targets and 2 moving. The two moving targets are moving with constant speed and direction through the center point of the image. One target is moving along track and the other is moving across track. Due to different focusing effects the target speeds have been chosen differently. The speed in along track is 0.5 m/s and the across track target is moving with 8 m/s at ground speed. The across track target is just a little bit unfocused, while the along track target is more unfocused. This is due to the relative speed v_{rel}. If the target ground speed is zero the relative speed will be the platform speed, and this speed is used as the SAR processing speed. If the target is moving along track it will influence the relative speed by $v_{rel} = v_p + v_t$, while for across track motion the relative speed will be $v_{rel} = \sqrt{v_p^2 + v_t^2}$. The relative speeds are in these cases 100.5m/s and 100.1m/s, respectively.

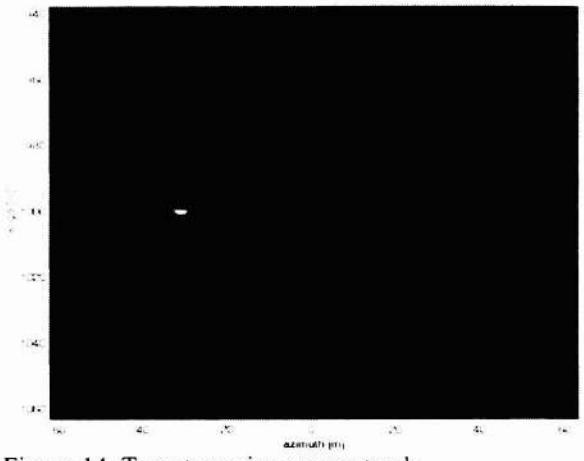

Figure 14. Target moving across track.

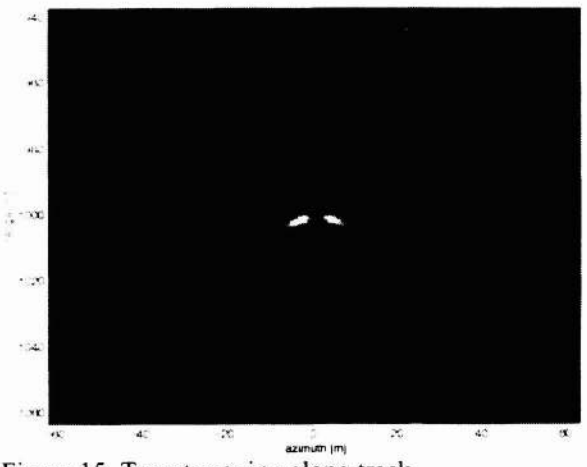

Figure 15. Target moving along track

If we SAR process one MTI filtered channel the two moving targets will appear clearly. However, the targets will be unfocused, because the relative speed is incorrect[6,7]. In Fig. 14 the MTI SAR image is shown. The signal from the across track target is much stronger than the along track target. The strength is dependent on the radial speed. The radial speed is maximum for the across track target at the shortest distance to the target and the speed decreases as the platform moves away from the target. For the along track target we have the opposite situation. If the across track target is removed the along track target will appear clearly, Fig. 15.

The along track moving target is already unfocused at speeds as low as 0.5 m/s. The range migration in this case is a hyperbola, but not at the assumed relative speed. The target will then be approximately focused for segments of different hyperbolas, and the target will unfocused. The radial speed is zero in the broadside direction and it increase as the Doppler

angle increases. This has the effect that after MTI filtered signal is zero at broad side and increases as the Doppler angle increases.

For the across track the relative speed error is smaller than for the along track target, even though the target speed is much higher. However, because minimum range distance to the target will occur at different azimuth position then the true azimuth position, the across track target will be placed an incorrect azimuth position.

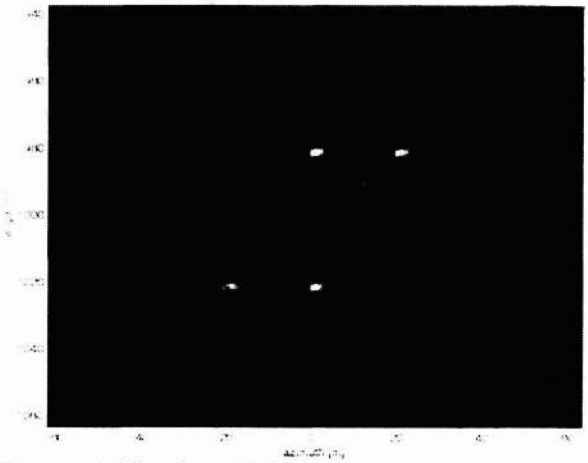

Figure 16. The clutter leakage

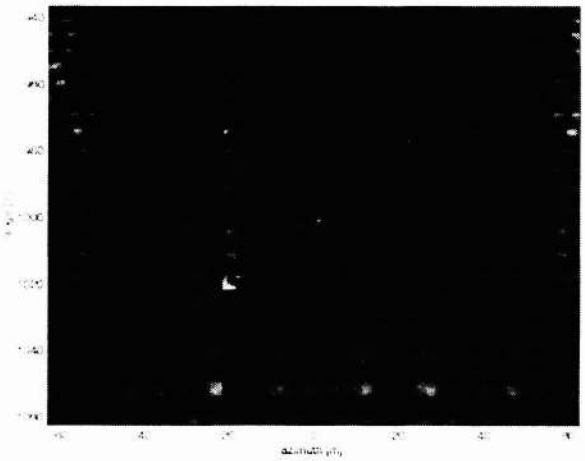

Figure 17. The nadir sidlobes

If both moving targets are removed we will see the performance characteristics off the MTI filter. The performance is limited by the antenna pattern, the bistatic configurations and the local backprojection assumptions. In Fig. 16 the MTI filtered SAR image over the same area as in Fig. 13, is shown. The image contains 9 subimages and depending on the target locations they will have different shapes and backscattering strength. The targets placed in the center of the subimages will have a signal strength dependent on the bistatic approximation while of center targets will depend on the local backprojection approximation. The suppression of the point targets, in this configuration is 50dB, and its performance is truly depending on the subimage size, as described in section 6.1. However, these effects are probably so small that the may be ignored in a real system.

The next step is to investigate the nadir sidelobe effects. If we assume that the nadir is 40 dB stronger than the point targets in the subimage the nadir sidlobes will pass the MTI-filter, according to section 6.2. In Fig. 17 this effect is shown. The simulation shows the bistatic case, but we have not included the scattering effects mention in section 4.

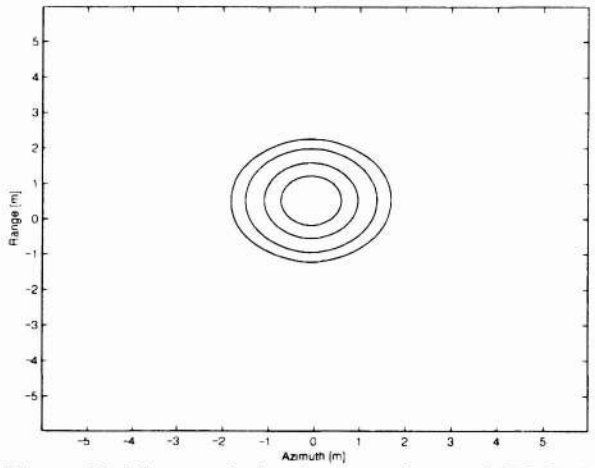

Figure 18. The correlation between the two MTI-SAR channels.

So far we have investigated the performance in one MTI-SAR channel which means that we have only used two antennas. If however the third channel is used there will be a time difference between these two channels. The time difference will case the moving targets to be separated. If we simulate a moving target, moving with 8 m/s in the across track direction a simple correlation between the channels will give Fig. 18.

From the correlation it is easy to determine the speed from correlation. The correlation offset is 0.5 meters which correspond to a speed of 5.3 m/s in the range plane, which is 8 m/s in the ground plane.

8. DISCUSSION

We will now discuss these VHF results and extract them to higher frequencies. Let us assume one radar working at UHF 200-900 MHz and one at microwaves 2-9 GHz. Let us ignore the system parameters and let us just discuss the bistatic results derived in this paper. The antenna separation is proportional to the wavelength, which means d_{ant}=4 at UHF and d_{ant}=0.4 for microwaves. The bistatic correction is proportional to the square of the antenna separation (4) while the signal from a moving target is dependent on the target movement between the two channels. For UHF the center frequency is increased 10 and therefore the movement decreased 10 times but the bistatic compensation has decreased 100 times. This means as we increase the frequency of the system the bistatic errors decreases.

As the wavelength gets smaller the ratio between the object size and the wavelength increases the bistatic scattering properties given in (14-15). This is compensated by the decreased ratio between the antenna separation and the distance. This means that the error cased by the large objects are the same for all frequencies. However at low frequency there will be very few large targets where (14) is valid, mostly the targets will act like point targets, which has a much broader backscattering lobe. This means that increased frequency increase amount of large targets.

9. CONCLUSIONS

We draw the conclusion that it is possible to build a UWB-WB GMTI SAR system, and that it can be made of bistatic antenna configurations. We have also discussed that we are free to do the MTI filtering in pulsed compressed data, in the SAR image or at stage in between as in the local backprojection.

At VHF the antenna beam is wide, and nadir is in the main lobe. The results indicate that the nadir will be one of the hardest issues to solve. Even if the scattering characteristics are the same for the nadir reflection in the different bistatic channels the sidelobes of the nadir will cause effect to the GMTI filter performance.

Another hard issue to solve, and maybe the most tricky one is the backscattering effects of large targets. If we use a maximum antenna separation of 40 meter at a distance of 1000 meter the scattering difference between the monostatic and bistatic could be -3 dB. However by increasing the distance to the target and by reducing the antenna separation it is possible to decrease this effect.

In comparison between different wavelengths: Low frequencies has the benefit to have few large targets much larger then the wavelength. High frequencies has the benefit of less bistatic compensation compared to the bandwidth. At VHF a target is large if the size is 10th of meters, at UHF meters and at microwaves decimeters. In forests there are not many objects that has the size of meters (for HH-pol), but a lot of objects that are decimeters. This means that we can use VHF probably UHF but probably not microwaves. For the bistatic compensation the maximum speed of the nadir is at VHF 2 m/s, UHF 0.2 m/s and microwaves 0.02 m/s. This means that we have no problems to use microwaves and probably UHF. From these arguments it seems that a UHF system is the best frequency to use for GMTI.

REFERENCES

1. J.H. Ender, "Detection and Estimation of moving target Signals by Multi-Channel SAR", AEU Int. J. Electron Commun. **50**, pp. 150-156, 1996
2. D.J. Coe and R.G. White, "Experimental Moving Target Detection Results from a Three-Beam Airborne SAR", AEU Int. J. Electron Commun. **50**, pp. 157-164, 1996
3. R.K. Raney, "Synthetic aperture imaging radar and moving targets", IEEE Trans. Aerospace Electron. Syst.. AES-7, pp 499-505, 1971
4. G. Smith and L.M.H. Ulander, "Forest Biomass Retrieval Using VHF SAR", Proc. 2nd Inter. Works. Retrieval of Bio- & Geo-physical Parameters from SAR Data for Land Applications, 1998, ESTEC, Noordwijk, The Netherlands
5. L.M.H. Ulander et. al., "Detection of Concealed Ground Targets in CARABAS SAR images using Change Detection", Proc. Algorithms for Synthetic Aperture Radar Imagery VI, SPIE 3721, Orlando, April 1999.
6. H. Hellsten and L.M.H. Ulander, "Airborne Array Aperture UWB UHF Radar-Motivation and System Considerations", Proc. 1999 IEEE Radar Conference, Massachusetts, April 1999
7. L.M.H. Ulander and H. Hellsten, "Low-frequency ultra-wideband array-antenna SAR for stationary and moving target imaging," *Proc. Radar Sensor Technology IV*, SPIE vol. 3704, Orlando, FL, 5-9 April 1999, (in press).
8. F.T. Ulaby et. al., *Radar Polarimetry for Geoscience Applications*, Artech House Inc., Norwood, 1990
9. O. Seger, M. Herbethson, and H. Hellsten, "Real Time SAR Processing of low Frequency Ultra Wide Band Radar Data", Proc. EUSAR'98, Fredrichhafen, Germany, 25-27 May 1998
10. L.E. Andersson, "Inversion Algorithms for Wide Band SAR Image Reconstruction" FOA Report C 30682-3.3, Swedish Defence Research Establishment, Sweden, 1992
11. M. Soumekh, "Bistatic Synhetic Aperture Radar Inversion with Application in Dynamic Object Imaging", IEEE Trans. Signal Proc. 9, pp 2044-2055, 1991
12. L.M.H. Ulander, "Performance of Stepped-Frequency Waveform for Ultra-Wideband VHF SAR", Proc. EUSAR'98, Fredrichhafen, Germany, 25-27 May 1998